An Inhomogeneous Background Imaging Method Based on Generative Adversarial Network

Xiuzhu Ye, *Senior Member, IEEE*, Yukai Bai, Rencheng Song, *Member, IEEE*, Kuiwen Xu, *Member, IEEE*, and Jianping An, *Member, IEEE*

***Abstract*— A deep learning-based inversion algorithm is developed to solve the inhomogeneous background inverse scattering problem (ISP). To alleviate the burden of nonlinearity and ill-posedness of the ISP, a noniterative method called the distorted-Born backpropagation scheme is introduced to quantitatively reconstruct a rough image of the unknown object in inhomogeneous background. The roughly reconstructed result serves as the input of the designed generative adversarial network (GAN), which outputs the fine reconstructed image of the relative permittivity. The generator network of the GAN is well designed as an encoder–decoder structure configured with the attention scheme. The discriminator network is taken to supervise the generator to learn the features of target scatterers through an adversarial training process. The proposed method is proven to be effective in reconstructing objects embedded in inhomogeneous background, which promises a real-time application future of the ISP.**

***Index Terms*— Image reconstruction, inverse problems.**

I. Introduction

MANY real-world problems such as nondestructive evaluation [1], [2], biomedical imaging [3], geophysical exploring [4], and microscopy [5], [6] can be considered as electromagnetic (EM) inverse scattering problems (ISPs). Such kind of problems usually involve using an EM transmitter to illuminate the region that cannot be seen by bare eyes, then the collected scattered field which contains information of unknown scatterer is analyzed numerically through imaging algorithms, in order to retrieve the spatial distribution of the EM properties of the scatterer. If all the multiple scattering effects are considered without approximation, ISP is capable of achieving super-resolution using just one single frequency data set [7]. Due to the high nonlinear relationship between the EM profile and the scattered field, the ISP is commonly solved as a nonlinear optimization problem. The cost function is iteratively updated which is consisted by the mismatch between the computed scattered field and the measured one. Furthermore, the ISP is commonly ill-posed [8], i.e., a slight change in the scattered field may cause a severe change in the reconstruction, and regularization schemes are, therefore, required to stabilize the optimization. The computational efficiency of most inversion algorithms is quite low due to the repeated calling of forward solver in each iteration, which prevent the further application of ISP in many real-time imaging scenarios.

Learning approaches successfully exceed traditional optimization methods in terms of speed. A well-trained neural network can give output in real time. Scientists in the field of ISP have taken advantage of learning approach a long time before deep learning approach is well-developed. As in the early stage, the computer was only capable of dealing with small-scale problem due to the limitation of the hardware. The learning-based inversion algorithms usually require prior information of the unknown scatterers, such as the shape or the EM properties, and only few parameters that describe the scatterers can be solved [9]–[11]. Modern deep learning approaches are capable of dealing with much larger amount of input and output data, which, therefore, offer the opportunity for developing deep learning-based imaging algorithms on the pixel level. This reveals a promising real-time application future for ISP.

A most straightforward solution is to treat the measured scattered field as the input and the reconstructed EM profile image as the output, where the neural network is trained as a black box without any physical knowledge included. However, the high nonlinearity and ill-posedness will reduce the generalizing ability of the neural network. Therefore, a major idea of the deep learning approach as applied in ISP is to cooperate as much physical insight into the neural network. Following this idea, the U-net convolutional neural network (CNN) was introduced to solve the pixel-based ISP by Wei and Chen [12] and Li *et al.* [13], where a rough image is got linearly from the scattered field by a backpropagation scheme (BPS) without iteration, and the neural network learns the nonlinear relationship between the rough image and the true image. This approach is proven to be more effective than

Manuscript received February 20, 2020; revised June 5, 2020 and July 13, 2020; accepted July 14, 2020. Date of publication August 24, 2020; date of current version November 4, 2020. This work was supported in part by the Natural National Science Foundation of China (NSFC) under Grant 61971036 and Grant 61971174; in part by the Fund of Key Laboratory for Information Science of Electromagnetic Waves (MoE) under Grant EMW201903; and in part by the Beijing Institute of Technology Research Fund Program for Young Scholars. *(Corresponding authors: Yukai Bai; Xiuzhu Ye.)*

Xiuzhu Ye and Jianping An are with the School of Information and Electronics Engineering, Beijing Institute of Technology, Beijing 100081, China (e-mail: xiuzhuye@outlook.com).

Yukai Bai is with the School of Electrical Engineering, Beihang University, Beijing 100083, China (e-mail: xiuzhuyenus@gmail.com).

Rencheng Song is with the School of Instrument Science and Opto-Electronics Engineering, Hefei University of Technology, Hefei 230009, China.

Kuiwen Xu is with the School of Information and Electronics Engineering, Hangzhou Dianzi University, Hangzhou 310008, China.

Color versions of one or more of the figures in this article are available online at http://ieeexplore.ieee.org.

Digital Object Identifier 10.1109/TMTT.2020.3015495

the direct solution, as the input and output are physically similar which fits the initial designing purpose of the U-net CNN. Guo *et al.* [14] have used machine learning method to learn the most time-consuming gradient calculation, and the ISP can also be solved in real time. Furthermore, Wei and Chen [15] have cooperated the whole CNN structure with the physical representation of the induced current, which is proven to be more effective in reconstruction.

In this article, a deep learning approach is introduced to solve the practical problem of imaging objects that are embedded in the inhomogeneous background. Inhomogeneous background problem is commonly encountered in through-wall imaging and nondestructive evaluation. The quality evaluation of the cores in optical fiber cable [16]–[18] is a typical example. Another example is the evaluation of the dielectric slab waveguide, where its core layer can be seen as unknown scatterer and the outer cladding layers are the background. Due to the multiple scattering between the background and the object, the problem is more difficult than imaging objects in the homogeneous background. There are several traditional iterative approaches developed to solve the inhomogeneous background ISPs. Such as in [19] and [20], the wall is considered as a known object and is excluded from update process. And in [21], a new differential equation is developed, and both the induced current and relative permittivity of the wall are excluded from update. As discussed before, all these iterative approaches suffer from low computational efficiency and slow imaging speed. Therefore, the proposed imaging method aims to overcome these drawbacks through using deep learning techniques.

To alleviate the burden of nonlinearity and ill-posedness of the ISP, a linear method called the distorted-Born backpropagation scheme (DB-BPS) is introduced to reconstruct a rough image of the unknown object in inhomogeneous background. This noniterative roughly reconstructed result serves as the input of the designed generative adversarial network (GAN), which outputs the fine reconstructed image of the relative permittivity. The generator network of the GAN is well constructed by introducing the object-attentional super-resolution blocks (OASRBs), where the attention scheme is realized by mask brunch. The advantages of the proposed method lie in the following points.

1) To the best of our knowledge, it is the first time that deep learning approach is applied in the inhomogeneous background ISP. The algorithm is capable of reconstructing the image in a very short time. If cooperating with a fast data acquisition equipment, it is possible to realize a real-time imaging which has a potential application in through-wall monitoring, emergency rescuing, and nondestructive evaluation.
2) A real-time linear inhomogeneous background algorithm is developed to retrieve the rough image of the relative permittivity. The method is developed based on the BPS by employing the distorted-Born approximation [22], [23], where inhomogeneous background, such as the wall components, is expressed by the inhomogeneous background Green's function. The rough images got by the proposed linear methods are taken as the input of the neural network. And the nonlinear relationship between the rough image and the fine true image is then learned by the neural network.
   It is noted that the subspace-based distorted-Born iterative method (S-DBIM) in [23] is proposed for homogeneous background case, which is a different scenario from the inhomogeneous background ISP. We borrow the idea of the inhomogeneous background Green's function as in S-DBIM to model the effect of the wall in this article. In S-DBIM, the updated profile in last iteration step is considered as the inhomogeneous background, while in the next step, the difference profile compared with the last step is considered as an unknown object embedded inside the inhomogeneous background. However, here in this article, the inhomogeneous background is a fixed term without updating, with the object embedded inside. In S-DBIM, the unknown induced current is retrieved through the singular value decomposition and nonlinear optimization, while in DB-BPS, the induced current is solved by a linear approximation with different formulas.
3) In this article, a GAN is constructed to solve the ISP, which is originally developed for super-resolution image recognition and it exactly fits the need of ISP. We developed a new frame of GAN where the attention scheme is added to further improve the resolution by highlighting the unknown scatterers and inhibiting the background and the unwanted artifacts.
4) To fit the need of real-world application, the method is able to reconstruct lossy scatterers (both real and imaginary parts of relative permittivity), while most of the existing literatures on machine learning-based ISPs only consider the real-valued relative permittivity. Numerical examples including the experimental data are given to prove the effectiveness and generalization of the proposed method.
5) In most contemporary literatures on machine learning-based ISPs, the training data set should contain similar shaped scatterers to the testing data set. In this article, the training data set is only the MNIST digits without adding any other shaped scatterers, while the testing profiles to be reconstructed can be cylindrical shaped scatters. This phenomenon reveals the strong generalization performance of the proposed GAN.

II. Forward Problem

In this article, the imaging of the concealed object embedded in inhomogeneous background is discussed. The 2-D experimental setup under transverse magnetic (TM) wave illumination is considered here. As depicted in Fig. 1, inside the square-shaped domain of interest D, the obstacle of relative permittivity ε_w surrounds the unknown scatterers. The shape and material of the obstacle are known *a priori*. The domain of interest is illuminated by N_i plane waves. Meanwhile, there are N_r antennas located at r_q^{s} with $q = 1, 2, \ldots, N_r$, which are expected to measure the scattered field produced by each incidence.

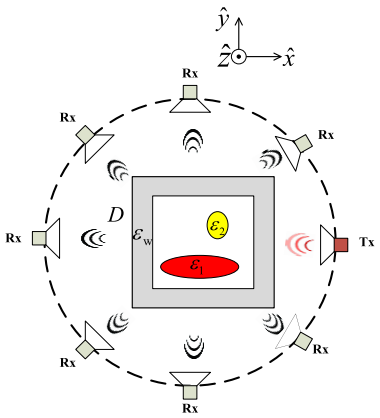

Fig. 1. Experimental configuration.

Before we move on to the inverse problem, we need to describe the forward problem which depicts the physical insights of the scattering effect. We use the method of moments (MOM) [24] with the pulse basis function and the delta testing function to discretize the domain D into $N = M \times M$ square subunits, and the centers of subunits are located at $r_1, r_2, \ldots, r_N$. The discretized form of total electrical field in domain D is denoted as vector $\overline{E}^{\text{tot}}$, with the field on the $n$thelement being $\overline{E}_n^{\text{tot}} = \overline{E}^{\text{tot}}(r_n)$. It satisfies the following discretized Lippmann–Schwinger equation [25]:

$$\overline{E}^{\text{tot}} = \overline{E}^{\text{inc}} + \overline{\overline{G}}_{\text{D}} \cdot \overline{\overline{\xi}} \cdot \overline{E}^{\text{tot}} \tag{1}$$

where $\overline{E}^{\text{inc}}$, $\overline{\overline{G}}_{\text{D}}$, and $\overline{\overline{\xi}}$ are the discretized incident electrical field, 2-D free space Green's function in domain D, and contrast function, respectively. The contrast $\overline{\overline{\xi}}$ is a diagonal matrix with the diagonal element $\overline{\overline{\xi}}(n,n) = \varepsilon_r(r_n) - 1$, where $\varepsilon_r(r_n)$ is the relative permittivity at r_n. If we discretize the domain of interest fine enough, each square subunit can be equivalent into a small circle of the same area. The equivalent radius of corresponding square subunit is denoted as a; then, we can obtain $\overline{\overline{G}}_{\text{D}}$ in the following formulas:

$$\overline{\overline{G}}_{\text{D}}(n,n') = \frac{ik_0\pi a}{2} J_1(k_0 a) H_0^{(1)}(k_0|\overline{r}_n - \overline{r}_{n'}|) \tag{2}$$

for $n \neq n'$, if $n = n'$, then

$$\overline{\overline{G}}_{\text{D}}(n,n') = \frac{ik_0\pi a}{2} H_1^{(1)}(k_0 a) - 1. \tag{3}$$

Here, $J_1(\cdot)$, $H_0^1(\cdot)$, and $H_1^1(\cdot)$ denote the first order of Bessel function, the zeroth order, and the first order of Hankel function of the first kind, respectively. k_0 is the wavenumber of homogeneous free space background. Note that $\overline{\overline{\xi}}(n,n)$ incorporate both the unknown scatterers and the known obstacles.

The induced current $\overline{J}$ is defined as

$$\overline{J} = \overline{\overline{\xi}} \cdot \overline{E}^{\text{tot}}. \tag{4}$$

According to (1), we can reformulate $\overline{J}$ as

$$\overline{J} = \overline{\overline{\xi}} \cdot \left(\overline{E}^{\text{inc}} + \overline{\overline{G}}_{\text{D}} \cdot \overline{J}\right). \tag{5}$$

The scattered field on the receivers outside the domain is given by

$$\overline{E}^{\text{sca}} = \overline{\overline{G}}_{\text{S}} \cdot \overline{J} \tag{6}$$

where $\overline{E}^{\text{sca}}$ and $\overline{\overline{G}}_{\text{S}}$ are $N_r \times 1$ and $N_r \times N$ dimensions, respectively, and $\overline{\overline{G}}_{\text{S}}$ is the Green's function which maps the current in domain D to the scattered field on the receivers.

III. Inversion Algorithm

The purpose of ISPs is to reconstruct relative permittivity distribution inside domain D, given the measured scattered field data. In this article, we aim to quantitatively reconstruct the relative permittivity of the scatterers enclosed by the inhomogeneous background such as a wall or obstacle. Even though the deep learning technique is powerful, the ISP is still too nonlinear and ill-posed for the neural network, which will reduce the generalization capability of the trained model. To alleviate the difficulty of the learning process, some retrievable prior information that depicts the physical process of scattering can be added into the neural network. Therefore, the deep learning-based inversion algorithm discussed in this article contains two major steps. The first step involves a noniterative linear inversion which retrieves the rough image of the relative permittivity from the knowledge of the scattering process (such as the predefined physical parameters $\overline{\overline{G}}_{\text{s}}$, $\overline{\overline{G}}_{\text{D}}$, and $\overline{E}^{\text{inc}}$). Then, this rough image serves as the input of the neural network which outputs the final reconstruction of the relative permittivity image.

A. Initialization: DB-BPS

The quality of input image has a clear impact on the output solution of neural network. We introduce a noniterative algorithm that will obtain preliminary nice results as the model inputs under the inhomogeneous background scenario. The basic idea follows the BPS as in [12]. However, the one introduced in [12] is a free space case while the one discussed in this article is designed for inhomogeneous background scenarios. It is linearized by applying the distorted-Born approximation method. The distorted-Born approximation method was first introduced by Chew and Wang [22], where the distorted-Born means that the total electric field is approximated by the total field produced by the inhomogeneous background by ignoring the one produced by the enclosed scatterer. Therefore, we name the proposed method as the DB-BPS.

Here, we consider the case of inhomogeneous background imaging. Instead of the free space Green's function $\overline{\overline{G}}_{\text{S}}$, $\overline{\overline{G}}_{\text{D}}$ as used in the homogeneous background case, we corporate the effect of the background into the inhomogeneous background Green's function which are denoted as $\overline{\overline{G}}_{\text{bS}}$ and $\overline{\overline{G}}_{\text{bD}}$, and the formulas are given as [23]

$$\overline{\overline{G}}_{\text{bS}} = \overline{\overline{G}}_{\text{S}} \cdot \left(\overline{\overline{I}} - \overline{\overline{\xi}}^{\text{bac}} \cdot \overline{\overline{G}}_{\text{D}}\right)^{-1} \tag{7}$$

$$\overline{\overline{G}}_{\text{bD}} = \overline{\overline{G}}_{\text{D}} \cdot \left(\overline{\overline{I}} - \overline{\overline{\xi}}^{\text{bac}} \cdot \overline{\overline{G}}_{\text{D}}\right)^{-1}. \tag{8}$$

Here, $\overline{\overline{\xi}}^{\text{bac}}$ denotes the inhomogeneous background contrast function and $\overline{\overline{I}}$ is the identity matrix. In the meantime, the total

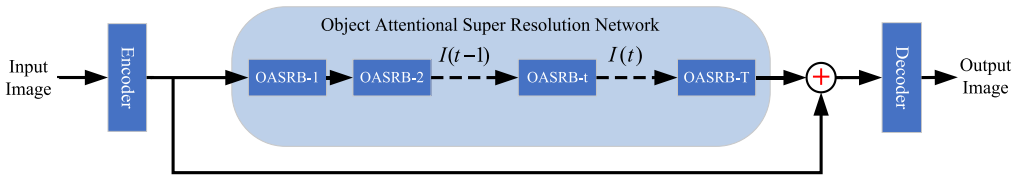

Fig. 2. Overall architecture of the generator.

electric field in the presence of the inhomogeneous background is denoted as $\overline{E}^{\text{bac}}$ and is calculated as

$$\overline{E}^{\text{bac}} = \left(\overline{\overline{I}} - \overline{\overline{G}}_{\text{D}} \cdot \overline{\overline{\xi}}^{\text{bac}}\right)^{-1} \cdot \overline{E}^{\text{inc}} \tag{9}$$

which can also be understood as the secondary incident field in the presence of inhomogeneous background. By ignoring the scattered field produced by the unknown objects, we approximate the total electric field in the domain to the secondary incident field produced by the inhomogeneous background. This linearization procedure can also be understood as the distorted-Born approximation

$$\overline{E}^{\text{tot}} = \overline{E}^{\text{bac}} + \overline{E}^{\text{sca}} \approx \overline{E}^{\text{bac}}. \tag{10}$$

We assume that the current produced by the unknown scatterer $\overline{J}^{\text{sca}}$ is linearly proportional to the back-propagated scattered field (produced by the unknown scatterer in presence of background)

$$\overline{J}^{\text{sca}} = \chi \cdot \overline{\overline{G}}_{\text{bS}}^{\text{H}} \cdot \overline{E}^{\text{sca}} \tag{11}$$

where the operator H denotes the Hermitian operation of the matrix and χ indicates the unknown complex coefficient to be determined.

A cost function is then constructed as the mismatch of the measured scattered field and the calculated one, which is the summation of the scattered field produced by inhomogeneous background and the unknown scatterers

$$F^{\text{obj}}(\chi) = \left\| \overline{E}^{\text{sca}} - \overline{\overline{G}}_{\text{S}} \cdot \overline{\overline{\xi}}^{\text{bac}} \cdot \overline{E}^{\text{bac}} - \overline{\overline{G}}_{\text{bS}} \cdot \left(\chi \cdot \overline{\overline{G}}_{\text{bS}}^{\text{H}} \cdot \overline{E}^{\text{sca}}\right) \right\|^2. \tag{12}$$

An analytical solution of χ can be obtained as

$$\chi = \frac{\left(\overline{E}^{\text{s}}\right)^{\text{T}} \cdot \left(\overline{\overline{G}}_{\text{bS}} \cdot \left(\overline{\overline{G}}_{\text{bS}}^{\text{H}} \cdot \overline{E}^{\text{s}}\right)\right)^*}{\left\| \overline{\overline{G}}_{\text{bS}} \cdot \left(\overline{\overline{G}}_{\text{bS}}^{\text{H}} \cdot \overline{E}^{\text{s}}\right) \right\|^2} \tag{13}$$

where $\overline{E}^{\text{s}} = \overline{E}^{\text{sca}} - \overline{\overline{G}}_{\text{S}} \cdot \overline{\overline{\xi}}^{\text{bac}} \cdot \overline{E}^{\text{bac}}$. With χ, the current produced by the unknown scatterers $\overline{J}^{\text{sca}}$ can be derived from (11); then, the total electric field can be numerated as

$$\overline{E}^{\text{tot}} = \overline{E}^{\text{bac}} + \overline{\overline{G}}_{\text{bD}} \cdot \overline{J}^{\text{sca}}. \tag{14}$$

For each incidence p, the relationship between the contrast of object $\overline{\xi}^{\text{obj}}$ and the current $\overline{J}_p^{\text{sca}}$ can be expressed as

$$\overline{J}_p^{\text{sca}} = \text{diag}\left(\overline{\xi}^{\text{obj}}\right) \cdot \overline{E}_p^{\text{tot}}. \tag{15}$$

An analytical solution can be obtained for each element in the domain of interest $\overline{\xi}^{\text{obj}}(n)$ with

$$\overline{\xi}^{\text{obj}}(n) = \frac{\sum_{p=1}^{N_i} \overline{J}_p^{\text{sca}}(n) \cdot \left[\overline{E}_p^{\text{tot}}(n)\right]^*}{\sum_{p=1}^{N_i} \left\| \overline{E}_p^{\text{tot}}(n) \right\|^2}. \tag{16}$$

B. Machine Learning Process

In the learning process, the preliminary reconstruction result of DB-BPS is treated as the model inputs, and the outputs are the true contrasts in the whole domain D. The GAN is composed of generator G and discriminator D networks, which are trained in an adversarial way until reaching a Nash equilibrium. The architecture of the proposed generator is, as depicted in Fig. 2, the inputs of which are the initial quantitative images of the contrasts that got by DB-BPS. The generator is composed of an encoder, a series of OASRBs, and a decoder. The target of the generator is to convert the rough input image into a fine reconstruction image.

There are two major requirements in solving the inhomogeneous background imaging ISP: 1) to distinguish the unknown scatterers from the inhomogeneous background and 2) super-resolution imaging requirement: to separate the adjacent scatterers by depressing the unwanted artifacts (due to the multiple scattering effect). Thus, in the design of the neural network, the pixels which belong to the unknown scatterers are expected to be retained and updated, while pixels that belong to the background and unwanted artifacts are expected to be suppressed or not updated. Therefore, according to the above requirements, we propose the generator network by introducing the spatial attention mechanism.

In this section, the structure of the GAN will be illustrated in detail. First, the modules of the generator are illustrated. Then, the structure of the discriminator is indicated. Finally, the training process is introduced.

1) Generator: Encoders: The initialized contrast got by the first step is fed into the model by a convolutional layer. The rough image of contrast is split into two channels: one corresponds to the real part and the other corresponds to the imaginary part of the relative permittivity profile. The two parts are stacked along the depth axes before being encoded. The encoding operation mixes the real part and the imaginary part together, by exchanging mutual information and retaining the inherent characteristics. The number of output channels is 64.

Object-Attentional Super-Resolution Network (OASRN): As shown in Fig. 2, our OASRN is constructed by cascading a series of OASRBs. All the OASRBs are identically structured.

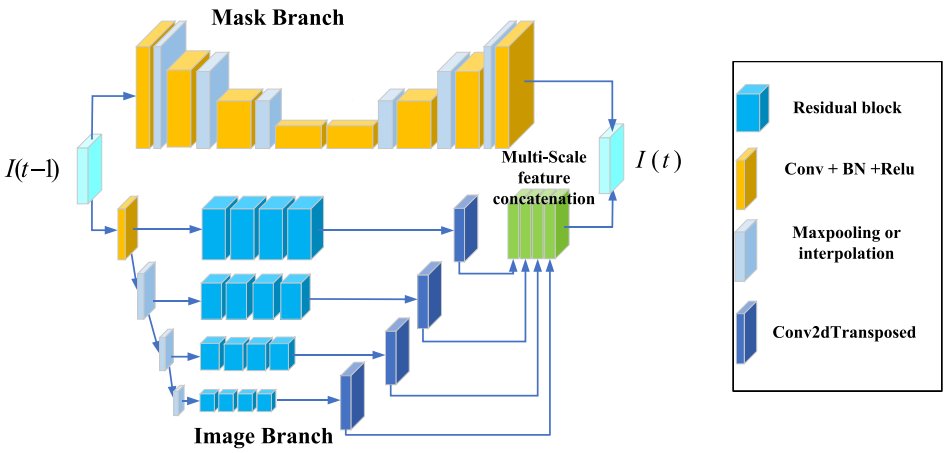

Fig. 3. Architecture of OASRB.

Each OASRB can be understood as one iteration step and the updated times of the rough contrast image equal to the number of OASRB modules. The OASRN gradually converts the rough image into fine image.

It is observed in Fig. 3 that each OASRB is consisted of two branches, which are called image branch and mask branch, respectively. The mask branch is marked according to both the value of dielectric constant and the positions of the objects and then the marking information is transferred to the image branch. By extracting the features of the image, the mask branch assists the image branch to further improve the quality of contrast image.

In the image branch, we applied the multi-scale fusion approach, which is inspired by the successful application of HRNet to realize the super-resolution human posture recognition [26]. Since our network is already composed of cascaded modules, unlike the HRNet where the multistage scale and depth keeps changing, our proposed module has only one constant stage. To extract features of the feature maps, the residual block retains the original features while capturing the crucial information, which is critical to the super-resolution task. At the final stage of the image branch, the low-scale features are amplified by deconvolution and connected with the maximum-scale features.

The mask branch inherits the structure of U-net, as depicted in Fig. 3 (the skip connections are omitted here for precision). To obtain the mask information and incorporate the values of dielectric contrasts and the positions of object, U-net CNN is used to process the input image. Let us assume that the input image of the tth OASRB is I_{t-1} and the output image is I_t. The object attention mask M_t is computed from the output values of U-net, which indicates the importance factor of each pixel in the image. The process of I_{t-1} by U-net can be expressed mathematically as

$$M_t = \sigma\left(\text{Unet}(I_{t-1})\right) \tag{17}$$

where σ is the sigmoid function. The object attention mask M_t is then transferred to the image branch and the image I_t is updated as

$$I_t = (1 + M_t) \odot (\text{MSF}(I_{t-1})) \tag{18}$$

where operator $\odot$ denotes an element-wise product and MSF denotes multiscale fusion effect. By applying the object attention masks to the image branch, the elements in the image I_t is either highlighted or inhibited.

In the inhomogeneous background ISP, the pixels which belong to the unknown scatterers are expected to be retained and updated, while pixels that belong to the background and unwanted artifacts are expected to be not updated. Therefore, in the mask branch, we mark importance with each pixel to decide whether it needs updating or not. The sigmoid activation function is adopted in the output layer to mark the importance of each pixel. And thus, the scatterer is automatically distinguished from the background with the artifacts suppressed. The mask generated by the attention mechanism will effectively guide the updating and optimization of the image branch. Therefore, the proposed network is able to fulfill the requirements in solving the inhomogeneous background ISP.

Decoder: At the last stage of OASRBs, the final outputs are fed into the decoder. The decoder is constructed by subpixel convolution layers as proposed by Shi *et al.* [27]. And the dimensions of the output image are four times to those of the original input image. The decoder contains two subpixel convolution layers, through which the image is magnified four times.

2) Discriminator: A discriminator network D is defined to train the generator, the goal of which is to distinguish the reconstructed image from the true one. The generator G is trained in order to fool the discriminator D. In such a process of adaptive adversarial training method, the two neural networks will be updated together until they reach a Nash-equilibrium. The above described process can be described mathematically as [28]

$$\min_{\theta_{\text{G}}} \max_{\theta_{\text{D}}} \mathbb{E}_{I^{\text{HR}} \sim p_{\text{GT}}(I^{\text{GT}})}\left[\log \text{D}_{\theta_{\text{D}}}\left(I^{\text{GT}}\right)\right] + \mathbb{E}_{I^{\text{LR}} \sim p_{\text{G}}(I^{\text{LR}})}\left[\log\left(1 - \text{D}_{\theta_{\text{D}}}\left(G_{\theta_{\text{G}}}\left(I^{\text{LR}}\right)\right)\right)\right]. \tag{19}$$

Here, $\text{G}_{\theta_{\text{G}}}$ is the generator parameterized by θ_{G} and $\text{D}_{\theta_{\text{D}}}$ indicates the discriminator network with parameter θ_{D}. I^{LR} is the input rough image, I^{GT} is the ground truth image for the

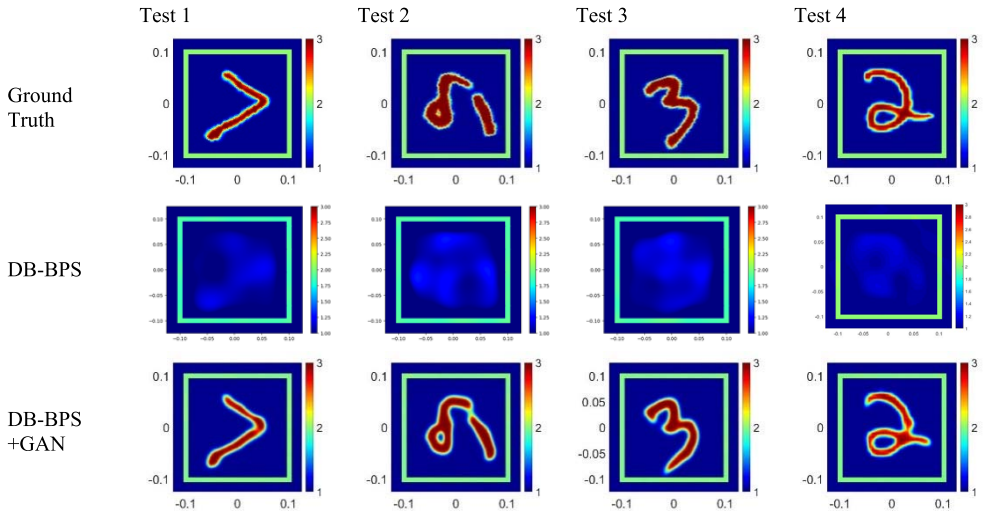

Fig. 4. Digital objects: reconstructed relative permittivity profiles from scattered fields with 10% noise for DB-BPS and GAN, where the relative permittivity is between 1.5 and 3. The first column shows the ground truth images for four representative tests.

training purpose, and $\mathbb{E}$ is the operator of the mathematical expectation. The discriminator network contains several convolutional layers and reduces the image dimensions by adjusting the step size of the convolution kernel. At the end of the discriminator, dense layer is used to merge spatial information into a vector and final activation function is a sigmoid function that outputs a probability of the classification.

3) Training Process: The generator loss function is denoted as

$$L_{\text{full}} = L_{\text{MSE}} + \alpha L_{\text{GAN}}^{\text{G}} \tag{20}$$

where $L_{\text{GAN}}^{\text{G}}$ denotes the adversarial loss, L_{MSE} indicates the mean square error (MSE), and α is a weighing parameter that represents the proportion of $L_{\text{GAN}}^{\text{G}}$ that accounts for the L_{full}. The pixel-wise MSE loss can be defined as

$$L_{\text{MSE}} = \frac{1}{LWH}\sum_{x=1}^{W}\sum_{y=1}^{H}\left(I_{x,y,z}^{\text{GT}} - \text{G}_{\theta_{\text{G}}}\left(I^{\text{LR}}\right)_{x,y,z}\right)^2 \tag{21}$$

where W, H, and L represent the width, height, and channels of the image, respectively.

It is well-known that GAN is difficult to train. In order to achieve a more stable training process, the least-square-based adversarial loss function for the generator is used as follows:

$$L_{\text{GAN}}^{\text{G}} = \mathbb{E}\left[\left(\text{D}_{\theta_{\text{D}}}\left(\text{G}_{\theta_{\text{G}}}\left(I^{\text{LR}}\right)\right) - 1\right)^2\right]. \tag{22}$$

For the discriminator, its loss function is defined as follows:

$$L_{\text{GAN}}^{\text{D}} = \frac{1}{2}\mathbb{E}\left[\left(\text{D}_{\theta_{\text{D}}}\left(I^{\text{GT}}\right) - 1\right)^2 + \left(\text{D}_{\theta_{\text{D}}}\left(\text{G}_{\theta_{\text{G}}}\left(I^{\text{LR}}\right)\right) - 0\right)^2\right]. \tag{23}$$

To make it clear, the discriminator tries to make the score of ground truth close to 1 and that of fake inputs close to 0. Notably, the balance between the MSE loss and adversarial loss is crucial when training GANs, which means an appropriate value α should be carefully chosen.

IV. Experiments

In this section, numerical examples including both the synthetic and experimental results are given to verify the effectiveness of the proposed method. In all the examples, 12 plane wave incidents that evenly distributed around a circle are used to illuminate the domain of interest. The size of domain of interest is $2\lambda \times 2\lambda$ and the frequency of the incident wave is 2.4 GHz. The obstacle is a square-shaped wall with outer side length 21 cm and thickness 1 cm. For each incidence, the scattered field is collected by 24 receivers which are evenly placed on the circle of radius 113 cm outside the domain of interest. Therefore, the dimension of the measured scattered field matrix $\overline{E}^{\text{sca}}$ is 24×12. The domain of interest is discretized into 40×40 square subunits. The synthetic forward data are added with 10% Gaussian white noise.

We use the MNIST data set for both training and testing. The training set is composed of 6000 samples, while the testing set is composed of 100 samples, which are of 10% samples randomly selected from the original MNIST data set. Each of the original digit image is resized from 28×28 into 40×40 for data preprocessing. ADAM optimizer is adopted for the generator and discriminator with $\beta_1 = 0.9$, $\beta_2 = 0.999$. Learning rate is initially set to1×10^{-4} and linearly decay to 0 after 20k iterations. We employed the trained MSE-based generator network as initialization before training the actual GAN to avoid unexpected local optima [29]. Our generator has three identical OASRBs and α for the adversarial loss is set to 1×10^{-3}. Maximum 20k iterations are set in the training process either to the pretrained generator or actual GAN.

A. First Example: Digital Objects

In the first example, the profiles of the embedded unknown scatterers are digital objects from MNIST data set. The digits from MNIST data set are set to be dielectric scatterers with random relative permittivity distributed between 1.5 and 3.0. The relative permittivity of the wall is 2. Some representative ground truth examples are presented in the first row of Fig. 4.

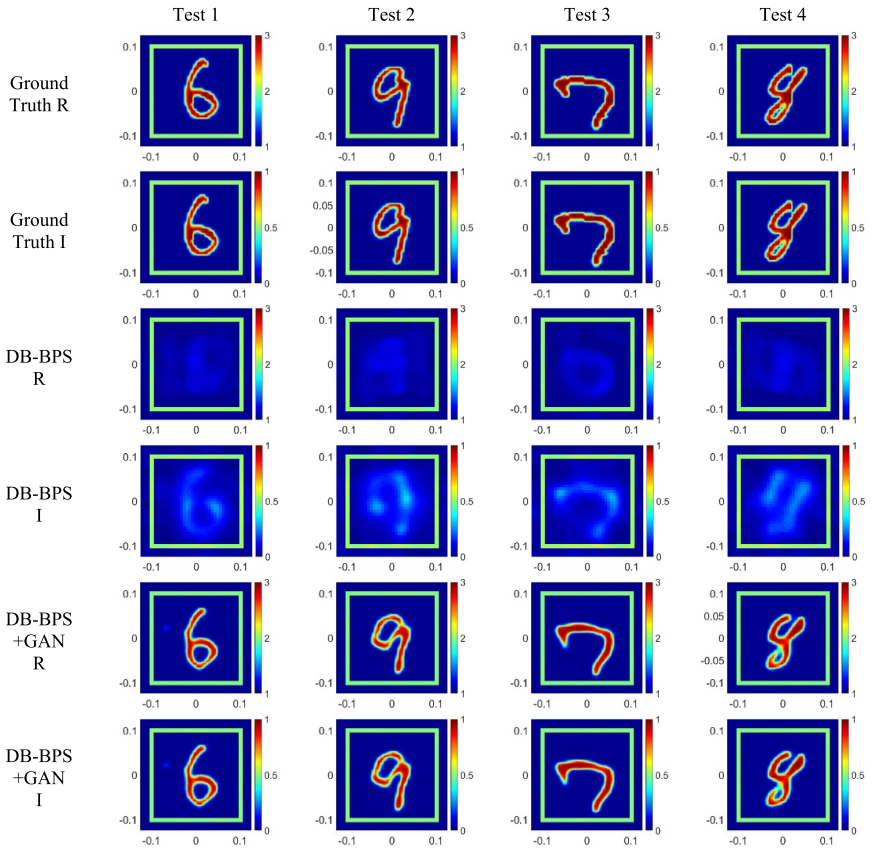

Fig. 5. Lossy digital objects: reconstructed relative permittivity profiles from scattered fields with 10% noise for DB-BPS and GAN, where the real part of the relative permittivity is between 1.5 and 3 and imaginary part is between 0 and 1. The first column shows the ground truth images for four representative tests, where the R stands for real part and I stands for imaginary part of the relative permittivity.

The rough image reconstructed by DB-BPS is shown in the second row of Fig. 4, where the reconstructed permittivity is relatively low due to the ignored multiple scattering effect. From the third row of Fig. 4, it is seen that satisfying fine reconstruction results are obtained by the proposed GAN method. The structural similarity (SSIM) index for the whole testing set is calculated as 0.9291.

B. Second Example: Lossy Digital Objects

In the second example, lossy digital objects are used to test the efficiency of the proposed method. The real part of the relative permittivity randomly ranges from 1.5 to 3 and the imaginary part ranges from 0 to 1. Here, the relative permittivity of the wall is $2 + 0.5i$. In Fig. 5, several testing experiments are presented where both the real and imaginary part are well reconstructed. The SSIM index for the whole testing set is calculated as 0.8946.

C. Third Example: Lossy "Austria" Profile

In the third example, we use the "Austria" profile as the unknown scatterers, which is shown in the first row in Fig. 6. It should be noted that there are no cylindrical scatterers used in the training process of the GAN (we used the MNIST digit data set), and this example serves as a test to the generalization ability of the trained GAN.

The centers for the two disks and the ring are $(0.2, 0.4)\lambda$, $(-0.2, 0.4)\lambda$, and $(0, -0.2)\lambda$, respectively. The radius of each disk is 0.15λ. The inner radius of the ring is 0.2λ and its outer radius is 0.4λ. The relative permittivity of the Austria profile is $3.0 + 0.9i$. The relative permittivity of the wall is $2 + 0.5i$.

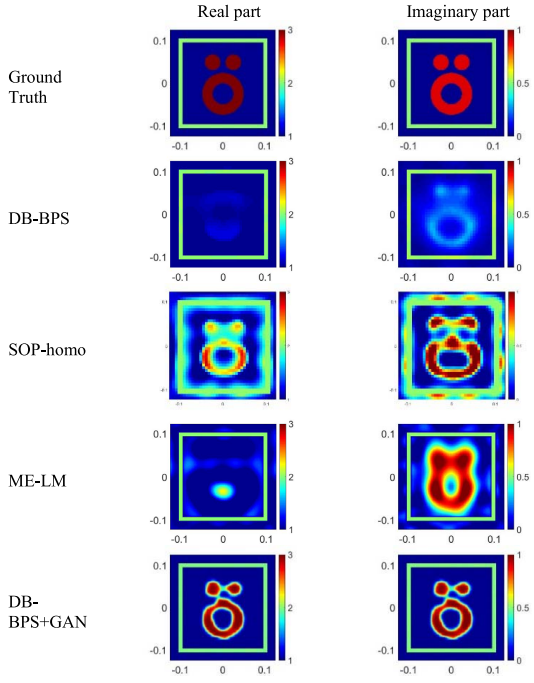

Fig. 6. Lossy "Austria" profile: reconstructed relative permittivity profiles from scattered fields with 10% noise for DB-BPS and GAN for "Austria" profile. The first column shows the ground truth images.

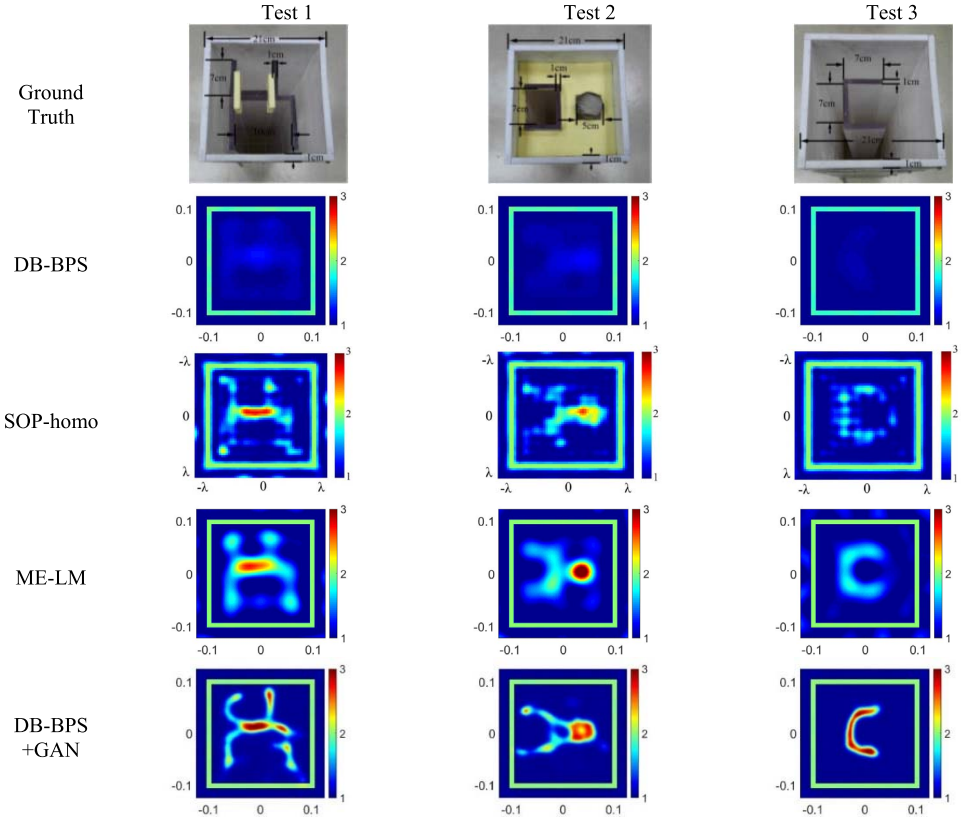

Fig. 7. Experimental results: reconstructed relative permittivity profiles from measured scattered field for DB-BPS and GAN. The first column shows the ground truth images for three representative tests.

Considering the effect of the wall and the complicated structure of the "Austria" profile, the effects of multiple scattering are very strong and consequently the reconstruction of through-wall case becomes much more difficult than all the previous experiments.

In Fig. 6, we present the reconstruction results and the comparison of it with the reconstruction result by the traditional method SOP-homo [19] and the modified enhanced Levenberg–Marquart (ME-LM) algorithm [30]. The ME-LM in [30] is tested only under a lossless scatterer case, and the result got by the lossy example here is worse than the lossless one. This phenomenon could be explained by the complexity of this lossy "Austria" example: 1) the real part of relative permittivity of the "Austria" profile in this article is higher than that in [30] (some parts in [30] are 2.8 instead of 3.0), which results in higher nonlinearity and 2) due to the lossy scatterers, e.g., the imaginary part of the relative permittivity, the wave decays quickly while passing through such scatterers, which raised more difficulty in the inversion.

The proposed machine learning method achieves super-resolution reconstruction for the details of the objects is clearly seen and the reconstructed contrast of the relative permittivity is accurate. The comparison of the proposed method and the traditional method is listed in Table I, where both the MSE and SSIM and the time used are listed, where we clearly see that the proposed method exceeds the SOP-homo and ME-LM in all aspects.

The DB-BPS takes some time when calculating $\overline{\overline{G}}_{\mathrm{bS}}$ and $\overline{\overline{G}}_{\mathrm{bD}}$, as in (7) and (8), there is matrix inversion involved.

TABLE I

COMPARISON OF MACHINE LEARNING-BASED METHOD AND THE TRADITIONAL METHODS

	Time/second	MSE	SSIM
DB-BPS	1.7143	/	/
GAN	0.0624	0.0506	0.8034
SOP-homo	5.4665	0.1480	0.3673
ME-LM	5.4827	0.3785	0.5544

This is inevitable for the inhomogeneous background case. In the real application scenario, such as through-wall imaging, the parameters of the wall are known *a priori*. Thus, $\overline{\overline{G}}_{\mathrm{bS}}$ and $\overline{\overline{G}}_{\mathrm{bD}}$ can be calculated only once and stored into the memory of computer. In such case, the DB-BPS process will be greatly accelerated without the time-consuming calculation of matrix inversion and the proposed algorithm would be real time.

D. Fourth Example: Experimental Results

To further verify the practicality of the proposed method, tests with experimental data have been conducted. In the configuration of the through-wall imaging system, the operating frequency is set as 2.4 GHz and there are 24 antennas evenly distributed on a circumference of a diameter of 113 cm, where 12 of them are used as transmitting antennas. The relative permittivity for the wall is 2 (Teflon). The relative permittivity of the cylindrical object is around 3, and the relative permittivity for U-shaped scatterers (plexiglass) is around 3. The ground truth dimensions of the objects are

labeled in Fig. 7. More configuration details can be found in [31]. It should be noted that in order to avoid interference of the near-field coupling effect, the two receiving antennas adjacent to the transmitting antenna are closed. Therefore, the final scattered field matrix is of dimension 21×12.

In Fig. 7, three representative experiments are reconstructed by the proposed method and comparison reconstruction results conducted by the traditional methods SOP-homo and ME-LM are shown in Fig. 7. The ground truth is depicted in the first row. From the reconstruction results, we can clearly see that there are less artifacts reconstructed by GAN comparing with the ones reconstructed by traditional iteration-based methods. And the relative permittivity reconstructed by the GAN is more accurate (as shown in the third example, where the ground truth relative permittivity is around 3).

We can conclude that the proposed machine learning-based method outperforms the traditional iteration-based methods in both reconstruction quality and computation efficiency.

V. Conclusion

This article proposed a deep learning-based method to solve the inhomogeneous background ISP. To alleviate the burden of nonlinearity and ill-posedness, a noniterative linear method based on the DB-BPS is proposed which is called DB-BPS. A primary good initial image of the contrast is reconstructed using DB-BPS, which serves as the input of the GAN. The generator network of the GAN is well constructed by introducing the OASRB module where the object attention scheme is realized by the proposed mask brunch. This GAN-based inversion is able to reconstruct super-resolution objects even with the surrounded wall.

The performance of all types of neural network relies on the training data set. One can never include all kinds of objects into the training data set. A good neural network should have a strong generalization ability even with a limited training data. The purpose of this article is to propose a method to solve the general inhomogeneous background ISP. The GAN-based inversion algorithm uses only MNIST data set in the training, without adding cylindrical or other artificial objects, and the reconstructed results by all kinds of scatterers (lossy scatterer, "Austria" scatterer, and experimental data) are still satisfactory and outperform the traditional method. Therefore, we conclude that the proposed method has a strong generalization ability. All the examples are reconstructed in almost real time. The machine learning approach incorporating with physical insight is proven to be effective in solving inhomogeneous background ISP. This reveals a promising future of the ISP for real-life application.

References

[1] S. Caorsi, A. Massa, and M. Pastorino, "A crack identification microwave procedure based on a genetic algorithm for nondestructive testing," *IEEE Trans. Antennas Propag.*, vol. 49, no. 12, pp. 1812–1820, Dec. 2001.

[2] D. L. Marks and D. R. Smith, "Inverse scattering with a non self-adjoint variational formulation," *Opt. Express*, vol. 26, no. 6, pp. 7655–7671, 2018.

[3] A. Abubakar, P. M. van den Berg, and J. J. Mallorqui, "Imaging of biomedical data using a multiplicative regularized contrast source inversion method," *IEEE Trans. Microw. Theory Techn.*, vol. 50, no. 7, pp. 1761–1771, Jul. 2002.

[4] M. Uecker, T. Hohage, K. T. Block, and J. Frahm, "Image reconstruction by regularized nonlinear inversion—Joint estimation of coil sensitivities and image content," in *Proc. 15th Annu. Meeting Int.-Soc.-Magn.-Reson.-Med./Eur.-Soc.-Magn. Reson.-Med.-Biol.*, Berlin, Germany, 2007, pp. 674–682.

[5] K. Belkebir and A. Sentenac, "High-resolution optical diffraction microscopy," *J. Opt. Soc. Amer. A, Opt. Image Sci.*, vol. 20, no. 7, pp. 1223–1229, Jul. 2003.

[6] T. X. Hoang, Y. B. Duan, X. D. Chen, and G. Barbastathis, "Focusing and imaging in microsphere-based microscopy," *Opt. Express*, vol. 23, no. 9, pp. 12337–12353, May 2015.

[7] T. Jun Cui, W. Cho Chew, X. X. Yin, Q. Jiang, and W. Hong, "Super resolution phenomenon in the detection of buried objects," in *Proc. IEEE Antennas Propag. Soc. Int. Symp. Dig. Held Conjunct USNC/CNC/URSI North Amer. Radio Sci. Meeting*, vol. 4, 2003, pp. 776–779.

[8] J. Hadamard, *Lectures on Cauchy's Problem in Linear Partial Differential Equations*. New Haven, CT, USA, 1923.

[9] M. R. Shaw, S. G. Millard, T. C. K. Molyneaux, M. J. Taylor, and J. H. Bungey, "Location of steel reinforcement in concrete using ground penetrating radar and neural networks," *NDT E Int.*, vol. 38, no. 3, pp. 203–212, Apr. 2005.

[10] M. R. Shaw, T. C. K. Molyneaux, S. G. Millard, M. J. Taylor, and J. H. Bungey, "Assessing bar size of steel reinforcement in concrete using ground penetrating radar and neural networks," *Insight-Non-Destructive Test. Condition Monitor.*, vol. 45, no. 12, pp. 813–816, Dec. 2003.

[11] M. I. Shimelevich and E. A. Obornev, "An approximation method for solving the inverse MTS problem with the use of neural networks," *Izvestiya, Phys. Solid Earth*, vol. 45, no. 12, pp. 1055–1071, Dec. 2009.

[12] Z. Wei and X. Chen, "Deep-learning schemes for full-wave nonlinear inverse scattering problems," *IEEE Trans. Geosci. Remote Sens.*, vol. 57, no. 4, pp. 1849–1860, Apr. 2019.

[13] L. Li, L. G. Wang, F. L. Teixeira, C. Liu, A. Nehorai, and T. J. Cui, "DeepNIS: Deep neural network for nonlinear electromagnetic inverse scattering," *IEEE Trans. Antennas Propag.*, vol. 67, no. 3, pp. 1819–1825, Mar. 2019.

[14] R. Guo, M. Li, F. Yang, S. Xu, G. Fang, and A. Abubakar, "Application of gradient learning scheme to pixel-based inversion for transient EM data," presented at the IEEE Int. Conf. Comput. Electromagn. (ICCEM), Mar. 2018.

[15] Z. Wei and X. Chen, "Physics-inspired convolutional neural network for solving full-wave inverse scattering problems," *IEEE Trans. Antennas Propag.*, vol. 67, no. 9, pp. 6138–6148, Sep. 2019.

[16] K. H. Jin, Y. G. Kim, S. H. Cho, J. C. Ye, and D. S. Yee, "High-speed terahertz reflection three-dimensional imaging for nondestructive evaluation," *Opt. Express*, vol. 20, no. 23, pp. 25432–25440, Nov. 2012.

[17] D. S. Yee, K. H. Jin, J. S. Yahng, H. S. Yang, C. Y. Kim, and J. C. Ye, "High-speed terahertz reflection three-dimensional imaging using beam steering," *Opt. Express*, vol. 23, no. 4, pp. 5027–5034, Feb. 23 2015.

[18] J. S. Yahng, C. S. Park, H. D. Lee, C. S. Kim, and D. S. Yee, "High-speed frequency-domain terahertz coherence tomography," *Opt. Express*, vol. 24, no. 2, pp. 1053–1061, Jan. 2016.

[19] X. Z. Ye, R. C. Song, and X. D. Chen, "Application of T-matrix method in solving mixed boundary separable obstacle problem," *Opt. Express*, vol. 22, no. 13, pp. 16273–16281, Jun. 2014.

[20] X. Ye, R. Song, K. Agarwal, and X. Chen, "Electromagnetic imaging of separable obstacle problem," *Opt. Express*, vol. 20, no. 3, pp. 2206–2219, Jan. 2012.

[21] K. Xu, Y. Zhong, X. Chen, and D. Lesselier, "A fast integral equation-based method for solving electromagnetic inverse scattering problems with inhomogeneous background," *IEEE Trans. Antennas Propag.*, vol. 66, no. 8, pp. 4228–4239, Aug. 2018.

[22] W. C. Chew and Y. M. Wang, "Reconstruction of two-dimensional permittivity distribution using the distorted born iterative method," *IEEE Trans. Med. Imag.*, vol. 9, no. 2, pp. 218–225, Jun. 1990.

[23] X. Ye and X. Chen, "Subspace-based distorted-born iterative method for solving inverse scattering problems," *IEEE Trans. Antennas Propag.*, vol. 65, no. 12, pp. 7224–7232, Dec. 2017.

[24] A. F. Peterson, S. L. Ray, and R. Mittra, *Computational Methods for Electromagnetics*. New York, NY, USA: IEEE Press, 1998.

[25] X. Chen, *Computational Methods for Electromagnetic Inverse Scattering*. Hoboken, NJ, USA: Wiley, 2018.

[26] K. Sun, B. Xiao, D. Liu, and J. Wang, "Deep high-resolution representation learning for human pose estimation," 2019, *arXiv:1902.09212*. [Online]. Available: http://arxiv.org/abs/1902.09212
[27] W. Shi *et al.*, "Real-time single image and video super-resolution using an efficient sub-pixel convolutional neural network," in *Proc. IEEE Conf. Comput. Vis. Pattern Recognit. (CVPR)*, Jun. 2016, pp. 1874–1883.
[28] I. Goodfellow *et al.*, "Generative adversarial nets," in *Proc. Adv. Neural Inf. Process. Syst.*, 2014, pp. 2672–2680.
[29] C. Ledig *et al.*, "Photo-realistic single image super-resolution using a generative adversarial network," in *Proc. IEEE Conf. Comput. Vis. Pattern Recognit. (CVPR)*, Jul. 2017, pp. 4681–4690.
[30] Y. Chu *et al.*, "Fast microwave through wall imaging method with inhomogeneous background based on Levenberg-Marquardt algorithm," *IEEE Trans. Microw. Theory Techn.*, vol. 67, no. 3, pp. 1138–1149, Nov. 2019.
[31] Q. Meng, D. Ye, J. Huangfu, C. Li, and L. Ran, "Experimental investigation on through-wall imaging based on non-linear inversions," *Electron. Lett.*, vol. 52, no. 23, pp. 1933–1935, Nov. 2016.

Xiuzhu Ye (Senior Member, IEEE) received the B.E. degree in telecommunication engineering from the Harbin Institute of Technology, Harbin, China, in 2008, and the Ph.D. degree from the Department of Electrical and Computer Engineering, National University of Singapore, Singapore, in 2012.

From 2012 to 2013, she worked as a Research Fellow with the Department of Electrical and Computer Engineering, National University of Singapore. Since 2013, she has been working as an Assistant Professor with Beihang University, Beijing, China. Since 2019, she has been an Associate Professor with the School of Information and Electronics, Beijing Institute of Technology, Beijing. Her research areas are electromagnetic inverse problems, microwave imaging methods, antenna designing, and machine learning.

Dr. Ye has served on review boards of various technical journals, including the IEEE TRANSACTIONS ON ANTENNAS AND PROPAGATION, the IEEE TRANSACTIONS ON MICROWAVE THEORY AND TECHNIQUES, *Radio Science*, and *Optics Express*.

Yukai Bai received the B.E. degree from the Taiyuan University of Technology, Taiyuan, China, in 2018. He is currently pursuing the M.S. degree at Beihang University, Beijing, China.

His current research interests include microwave imaging and electromagnetic inverse scattering problems.

Rencheng Song (Member, IEEE) received the B.S. degree in mathematics from Jilin University, Changchun, China, in 2005, and the Ph.D. degree from Zhejiang University, Hangzhou, China, in 2010.

He is currently an Associate Professor with the Department of Biomedical Engineering, Hefei University of Technology, Hefei, China. His research interests include intelligent perceptions for biomedical measurements, such as video-based physiological parameter measurement, electromagnetic imaging, and machine learning.

Kuiwen Xu (Member, IEEE) received the B.E. degree from Hangzhou Dianzi University, Hangzhou, China, in 2009, and the Ph.D. degree from Zhejiang University, Hangzhou, in 2014, all in electrical engineering.

From 2012 to 2013, he was a Visiting Ph.D. Student with the National University of Singapore, Singapore. From 2014 to 2015, he was a Senior Researcher with Huawei Technologies Co., Ltd., Hangzhou. He was invited to the State Key Laboratory of Terahertz and Millimeter Waves, City University of Hong Kong, Hong Kong, as a Visiting Professor, in 2018. Since September 2015, he has been with Hangzhou Dianzi University, where he is currently an Associate Professor. His research interests include electromagnetic inverse problems, microwave measurement, and novel antenna design.

Jianping An (Member, IEEE) received the Ph.D. degree from the Beijing Institute of Technology, Beijing, China, in 1996.

He joined the School of Information and Electronics, Beijing Institute of Technology, in 1995, where he is currently a Full Professor and also the Dean of the School of Information and Electronics. His research interests include digital signal processing, wireless communications, and satellite networks.

Dr. An has received two national awards for technological inventions and science and technology progress.